Development and application of laser induced incandescence (LII) as a diagnostic for soot particulate measurements

Snelling, David; Gareau, Daniel; Fetter, D.; Medlock, J.; Campbell, Ian; Gulder, O.

Development and application of laser induced incandescence (LII) as a diagnostic for soot particulate measurements.

D. R. Snelling, D. R. Gareau, D. Fetter, J. E. Medlock, I. G. Campbell, and Ö. L. Gülder,
National Research Council of Canada, Montreal Road, Ottawa, Ontario.

Introduction

Soot volume fraction measurements are important for studies of soot formation and radiation processes in flames, and for monitoring post-flame gases. Light extinction is widely used as a diagnostic technique but suffers from the drawback of measuring a line-of-sight average, and while tomographic reconstruction can be used to calculate soot profiles in radially symmetric flames, this is not generally possible. Laser induced incandescence (LII) has emerged as a promising technique for measuring spatially and temporally resolved soot volume fraction in flames[1-7]. In LII the soot is heated to incandescence by a short duration laser pulse. With sufficiently high laser energies the soot particles reach temperatures of 4000-4500 K and the resultant radiation, which is blue shifted from the normal soot flame radiation and is of short duration, can readily be detected. LII typically has a temporal resolution of 10 ns and can be used to perform both point measurements and 2-D planar visualization.

In this paper we describe our development of the LII technique for point measurement in flames and the calibration of the technique using a simple laminar diffusion flame. Since LII provides only relative soot volume fraction measurements, an absolute calibration is necessary. The radial soot volume fraction profiles in the laminar diffusion flame were measured by Abel inversion of line-of-sight attenuation measurements at 532 and 1064 nm. We have implemented a numerical model of the LII processes to aid in the interpretation of experimental results. A description of the LII technique and its calibration are discussed. The application of LII to a confined C_3H_8/air diffusion flame and some results of the model predictions and their comparison to experiment will be included in the presentation.

Experimental

The laminar diffusion flame used in these experiments was similar to that used by Gülder[8] except that the fuel tube was 13.9 mm. The C_2H_4 flow rate was 3.27 cm^3/min and the surrounding air flow rate 170 SLPM. The visible flame height was 67 mm. The schematic of the LII setup is shown in Fig. 1. A Continuum Surelite1 Nd:YAG laser was modified by including an aperture in the laser cavity to improve the beam quality. This reduced the maximum energy to 40 mJ and the energy delivered to the flame was varied with a half wave plate to control the polarisation and a polariser to pass only vertically polarised light. The laser was focussed to a sheet with Gaussian parameters ($1/e^2$ full width) of 3.62 and 0.44 mm. The LII signal from the centre of the laser sheet was imaged at 2:1 magnification with a 54 mm diameter lens of 190 mm focal length onto an apertures of 1.06 mm in front of the photomultipliers (PM's). Thus the volume of the flame viewed was a cylinder of diameter 0.53 mm whose length was the width of the laser sheet (0.44 mm). The LII signal was split 50:50 between two PM's each equipped with an interference filter centred at 455.5 nm with a bandwidth of 11.0 nm. One of the PM's was connected directly to a gated integrator whose gate width was set at 25 ns to measure the peak of the LII signal (subsequently referred to as the peak signal). The other PM was connected to a charge-coupled amplifier which measured the total charge collected during the LII pulse and thus measured the time integrated LII signal.

For the 532 and 1064 nm laser attenuation experiments a 3 times beam expander followed by a 1 m focal length lens was used. At 1064 nm the focal beam diameter in the flame, ω_0, was 0.24 mm (Gaussian $1/e^2$ diameter); and the confocal parameter (total distance between the points at which the beam had grown to ($\sqrt{2}$. ω_0) is 160 mm, ensuring that there was little increase in beam size over the maximum flame diameter of 6 mm. A beam splitter directed part of the pre-flame laser beam on to a silicon photodiode detector (detector A) and the transmitted laser beam was measured with a second detector (B). Signals from both detectors were detected with gated integrators whose outputs were ratioed to give A/B. In this way we were able to correct for small changes in laser power and the flame transmission could be measured to an accuracy of ~0.25%. The transmission measurements were made every 0.1 mm across the flame.

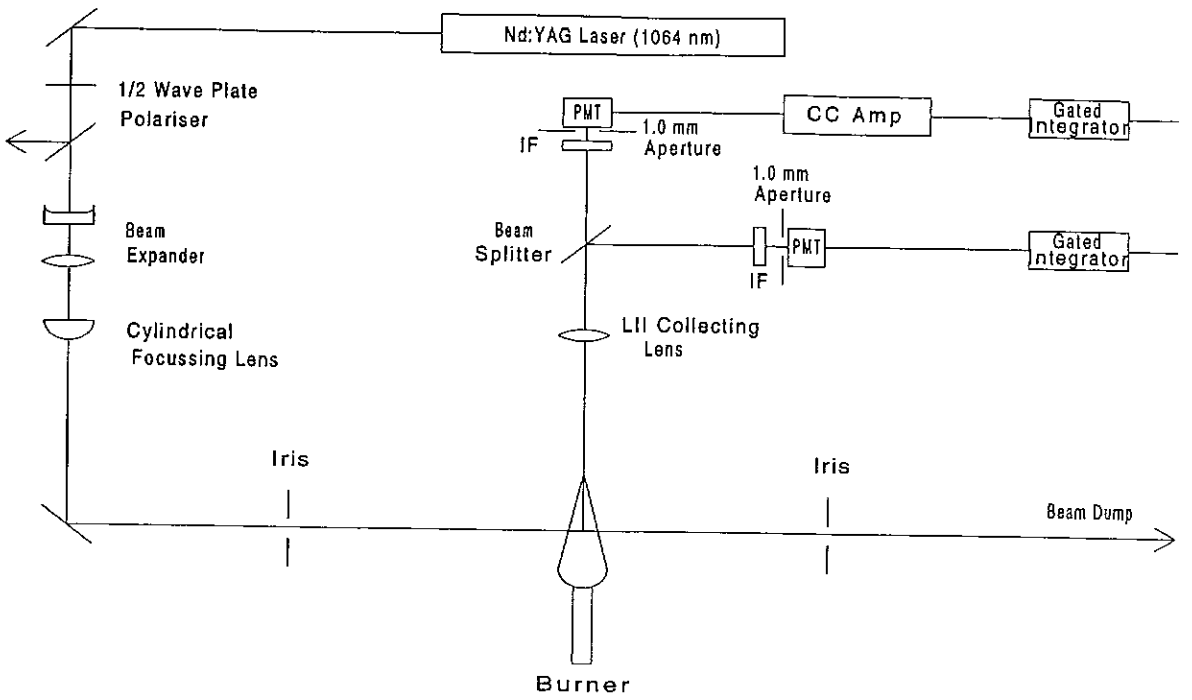

Results and analysis

In the Rayleigh limit the soot volume fraction, f_v, is given by

$$f_V = \frac{\ln(\tau).\lambda}{6.\pi.L.E(m)}$$

Where τ is the flame transmission, λ the wavelength and L the flame width. The complex refractive index is m and $E(m) = -\mathrm{Im}\{(m^2-1)/(m^2+2)\}$ thus

$$m = n + ik$$

$$E_m = \frac{6nk}{(n^2 - k^2 + 2)^2 + 4n^2k^2}$$

Using data from Dalzell and Sarofim[9]:
at 532 nm m=1.59+0.58i and E(m)=0.264; at 1064 nm m=1.63 + 0.7i and E(m)=0.303

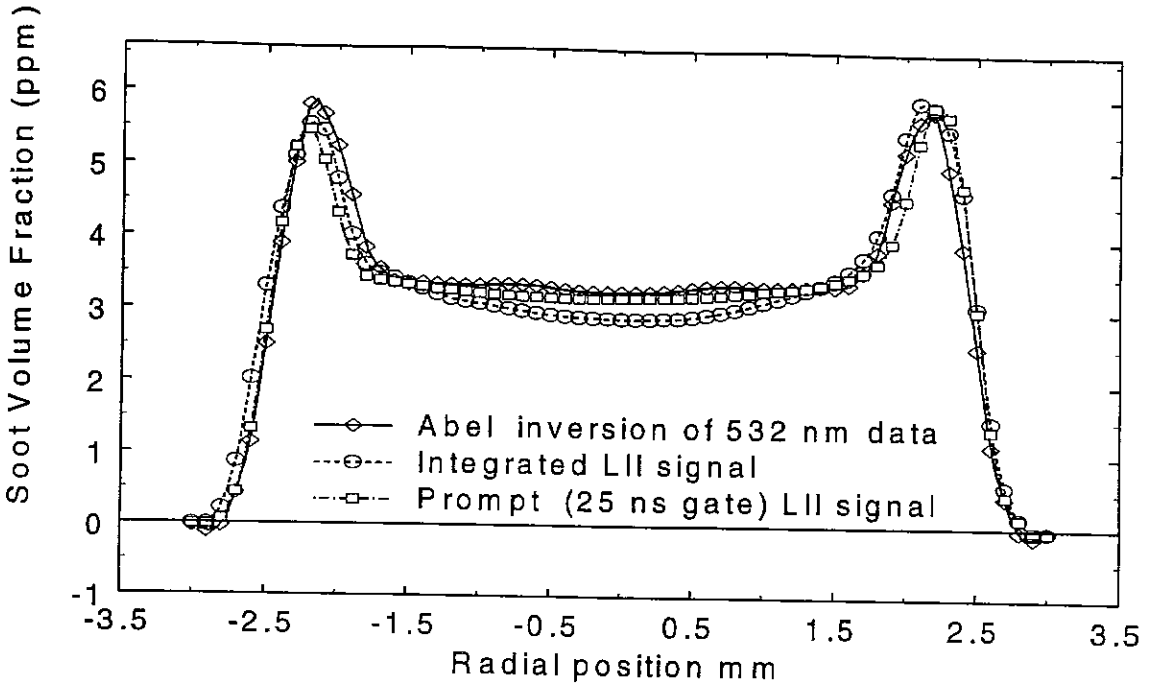

Figure 2 Comparison of prompt and integrated LII signal with soot volume fraction measured by Abel inversion of 532 nm transmission data.

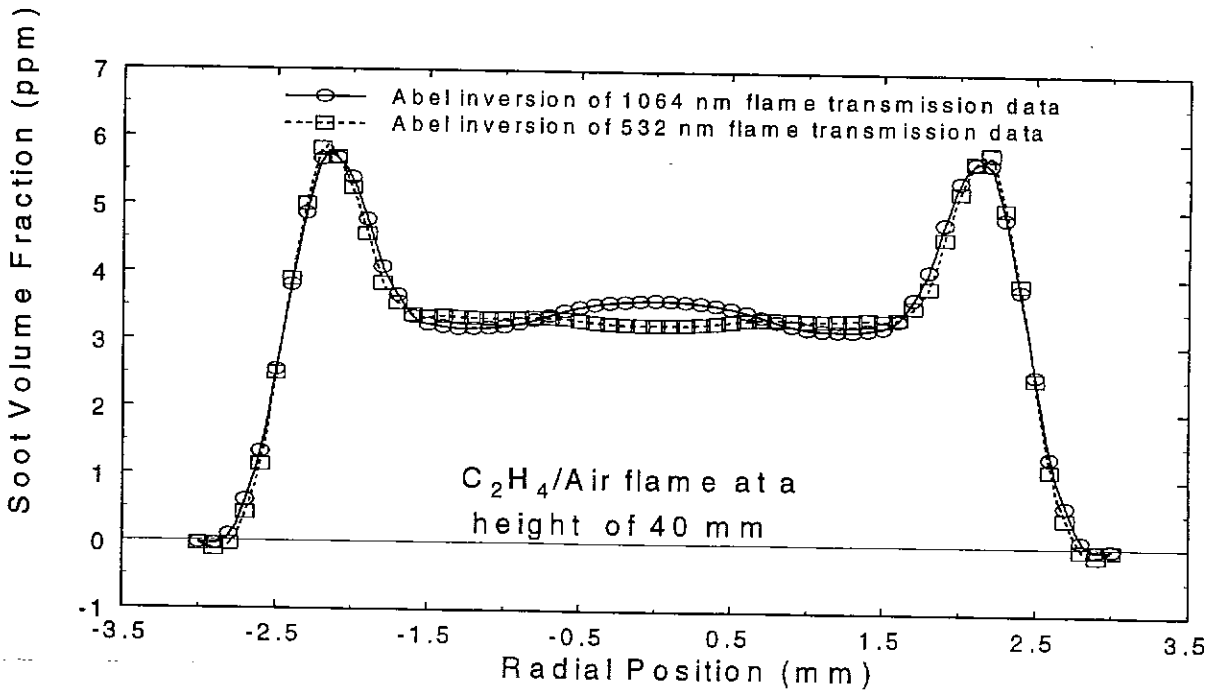

Figure 3 Radial profiles of soot volume fraction from Abel inversion of laser transmission measurements

The Abel inversion of the transmission measurements was performed using the 3 point Abel algorithm of Dasch[10] with a data spacing of 0.2 mm. The resultant curves are shown in Fig.2, where it can be seen that there is generally very good agreement between the 532 nm and 1064 nm data.

LII measurements were performed at the same location in the laminar difussion flame. When the energy of the 1064 nm laser is increased above LII detection threshold there is an initial sharp increase in LII signal. With a laser energy of 4 mJ a further increase in energy produces very little increase in LII signal. The LII detection is typically operated in this plateau region[3-6] and we have used a laser energy of 6 mJ for our LII measurements which are shown in Fig.3 with the 532 nm Abel inverted data for comparison.

In fig. 3 the LII data has been scaled to the Abel data so that the integrated soot volume fraction over the total flame width is constant for all the curves. In general it can be seen that there is good agreement between the soot profiles from LII and Abel inverted transmission measurements, with the prompt LII signal following the Abel data more closely.

Numerical model of soot heating.

The numerical modelling of the transient heating and subsequent radiation of soot particles exposed to short duration (10 nsec) laser pulses is described below. The equations are presented for soot particles considered as equivalent spheres, an approach that has been almost exclusively been followed in the LII literature.

The heat transfer energy balance equation is [2,11]:

$$C_a q - \frac{2 K_a (T-T_0) \pi D^2}{(D + G \lambda)} + \frac{H_v}{M_V} \frac{DM}{Dt} + q_{rad} - \frac{1}{6} \pi D^3 \rho_S c_s \frac{DT}{Dt} = 0 \qquad (1)$$

$C_a q$ is the absorbed laser energy, where in the Rayleigh limit, the absorption cross section C_a is given by:

$$C_a = \frac{\pi^2 D^3 E(m)}{\lambda} \qquad (2)$$

The second term involves heat transfer to the surrounding medium for a particle in the transition regime between continuum and free molecule (Knudsen) heat transfer. Since the mean free path in the gas is typically much larger than the soot particle diameter the particle is largely in the free molecule limit and the heat transfer coefficient is independent of particle size. G is a geometry dependent heat transfer factor[12], equal to $8f/[\alpha(\gamma+1)]$ where $\gamma=C_P/C_V$ (= 1.40 for air), f is the Euken factor (5/2 for monatomic species), α is the accomodation coefficient ≈ 0.9 .

The third term is heat loss due to evaporation of the soot and is given by:

$$\frac{dM}{dt} = \frac{\rho_s}{2} \pi D^2 \frac{dD}{dt} = - \pi D^2 \frac{N_{AV} \frac{P^*}{R T_V} \exp[\frac{\Delta H(T-T^*)}{R T T^*}]}{\frac{1}{\beta}(\frac{2\pi M_V}{R T_S})^{1/2} + \frac{D}{2 D_{AB}}} \qquad (3)$$

Again the flux of carbon vapour is dominated by the free molecule regime (the first term in the denominator of Eqn. 3) and is independent of particle size. The radiation term can be approximated as:

$$q_{rad_p} = 4\pi^2 D^3 \sigma_{SB} T^4 \left(\frac{E(m)}{\lambda} \right)_{600} \qquad (4)$$

Does heat loss occur at all wavelength or only at the laser's wavelength ?

where the expression in parentheses is evaluated at some average wavelength, 600 nm in our case. Heat loss due to radiation is unimportant compared to all the other heat loss terms. These equations constitute a coupled set of

differential equations for D and T that have been solved numerically using a Runge-Kutta integration routine.

If we consider the soot particles, more realistically, as soot agglomerates made up of N_P uniform, just-touching primary spherical particles of diameter d_p, then the terms in D^2 and D^3 in the numerators of Eqns. 1-4 can be replaced by $N_p d_P^2$, and $N_p d_P^3$, respectively. The diameter particle dependence in the denominator of Eqn. 1 and 3 reflect the dependence of heat transfer and the flux of evaporating soot on this quantity in the continuum limit. For soot particles these terms are small and are dominated by the free molecule

The results reported here and measurements of the LII decay curves and their comparison to the predictions of a numerical model of the soot heating and Radiation processes will be discussed during the presentation .

Glossary of Terms

C_a	.soot particle absorption cross section (m^2)
C_S	-specific heat of carbon (see Melton 1.90 $Jg^{-1}K^{-1}$)
C_V	-specific heat of air in J/Kg.K
D	-soot particle diameter (m)
D_{AB}	-interdiffusion coefficient for soot vapour into surrounding gas (m^2/s)
f	-Eucken factor (5/2 for monatomic species)
G	-geometry dependent heat transfer factor $G=8f/(\alpha(\gamma+1))$
H_V	-heat of vaporisation of carbon, $7.78x10^5$ J/mol
K_a	-thermal conductivity of ambient air $(5.83x10^{-5}(T_o/273)^{0.82}$ at temperature T_o
K_n	-Knudsen number $K_n=\lambda /D$
M_V	-molecular weight carbon vapour gm/mole
M_A	-molecular weight of air gm/mole
M	-mass of carbon (kg)
n_V	-molecular number density at soot particle surface, $n_V=n.X_{VS}$ (m^{-3})
N_{av}	-Avogadro's number (/mole)
N_V	-total soot molecular flux (m^2/s)
P	-pressure of soot vapour (N/m^2)
P^*	-reference pressure (N/m^2)
q	-laser fluence (J/cm^2)
T	-soot surface temperature
T^*	-reference temperature (K)
T_0	-gas temperature
T_S	-soot surface and vapour pressure
X_{VS}	-mole fraction of soot vapour at particle surface
α	-accommodation coefficient (approximately 0.9)
β	-evaporation coefficient
γ	$-\gamma=C_P/C_V$ (=1.4 for air)
λ	-mean free path, $\lambda=1/(2^{0.5}\pi(\sigma_{AB})^2$ in rigid sphere approximation (m).
ρ_s	-density of soot (kg/m^3)
σ_{SB}	-Stefan-Boltzmann constant

References

1.) Dasch, C.J. Continuous-wave probe laser investigation of laser vaporization of small soot particles in a flame. Applied Optics 23, 2209-15 (1984)

2) Melton, L.A. Soot diagnostics based on laser heating. Applied Optics 23, 2201-8(1984)

3) Quay, B., Lee, T.W., Ni, T. & Santoro, R.J. Spatially resolved measurements of soot volume fraction using laser-induced incandescence. Combustion and Flame 97, 3-4 (1994)

4)Shaddix, C.R. & Smyth, K.C. Soot production in flickering methane, propane, and ethylene diffusion flames. Chem. Phys. Processes Combust 329-32 (1994)
5) Vander Wal, R. L. & Weiland, K. J. Laser-induced incandescence: Development and characterization towards a measurement of soot-volume fraction. Applied Physics B 59, 445-452 (1994)
6.)Bengtsson, P.E. & Alden, M. Soot-visualization strategies using laser techniques. Laser-induced fluorescence in C2 from laser-vaporized soot and laser-induced soot incandescence. Appl. Phys. B: Lasers Opt 1, 51-9 (1995)
7)Will, S., Schraml, S. & Leipertz, A. Two-dimensional soot-particle sizing by time-resolved laser-induced incandescence. Optics Letters 20, 2342-4 (1995)
8)Gulder, O.L. Influence of hydrocarbon fuel structural constitution and flame temperature on soot formation in laminar diffusion flames. Combust Flame 78, 179-194 (1989)
Megaridis, C.M. & dobbins, R.A. Comparison of soot growth and oxidation in smoking and non-smoking ethylene diffusion flames. Combustion Science And Technology 1989 66, 1-16 (1989)
9)Dalzell, W.H. & Sarofim, A.F. Optical constants of soot and their application to heat flux calculations. Journal of Heat Transfer v 91, 100-104 (1969)
10) Dasch, C.J. One-dimensional tomography: a comparison of Abel, onion-peeling, and filtered backprojection methods. Applied Optics 31, 1146-52 (1992)
11)Hofeldt, D.L. in International Congress and Exposition, San Francisco, California. (Society of Automotive Engineers, SAE paper 930079 1993)
12)McCoy, B.J. & Cha, C.Y. Transport phenomena in the rarefied gas transition regime. Chemical Engineering Science 29, 381-388 (1974)

F. Lin

The Combustion Institute
Canadian Section

1997 Spring Technical Meeting

25 to 28 May
DalTech
Halifax, NS